minerals

MDPI

Article

Mineralization and Structural Controls of the AB-Bid Carbonate-Hosted Pb-Zn (±Cu) Deposit, Tabas-Posht e Badam Metallogenic Belt, Iran

Abdorrahman Rajabi [1,*], Carles Canet [2], Pura Alfonso [3,*], Pouria Mahmoodi [4], Ali Yarmohammadi [4], Shahba Sharifi [1], Amir Mahdavi [5] and Somaye Rezaei [6]

[1] School of Geology, College of Science, University of Tehran, Tehran 1417614411, Iran; Shahba.sharifi@ut.ac.ir
[2] Instituto de Geofísica, Universidad Nacional Autónoma de México, Coyoacán, Mexico City 04150, Mexico; ccanet@igeofisica.unam.mx
[3] Departament d'Enginyeria Minera, Industrial i TIC, Universitat Politècnica de Catalunya, Av. de les Bases de Manresa 61–73, 08242 Manresa, Spain
[4] Department of Geology, Faculty of Sciences, Tarbiat Modares University, Tehran 14115111, Iran; airop1365@gmail.com (P.M.); yarmohammadi77ir@yahoo.com (A.Y.)
[5] Department of Geology, Faculty of Sciences, University of Birjand, Birjand 9717434765, Iran; am.mahdavi@birjand.ac.ir
[6] Ravar Kooshan Industrial and Mining Company, Kerman 7651613556, Iran; s.rezaei2632@gmail.com
* Correspondence: rahman.rajabi@ut.ac.ir (A.R.); maria.pura.alfonso@upc.edu (P.A.)

Citation: Rajabi, A.; Canet, C.; Alfonso, P.; Mahmoodi, P.; Yarmohammadi, A.; Sharifi, S.; Mahdavi, A.; Rezaei, S. Mineralization and Structural Controls of the AB-Bid Carbonate-Hosted Pb-Zn (±Cu) Deposit, Tabas-Posht e Badam Metallogenic Belt, Iran. *Minerals* **2022**, *12*, 95. https://doi.org/10.3390/min12010095

Academic Editors: Huan Li and Han Zheng

Received: 10 December 2021
Accepted: 5 January 2022
Published: 14 January 2022

Publisher's Note: MDPI stays neutral with regard to jurisdictional claims in published maps and institutional affiliations.

Abstract: The Ab-Bid deposit, located in the Tabas-Posht e Badam metallogenic belt (TPMB) in Central Iran, is the largest Pb-Zn (±Cu) deposit in the Behadad-Kuhbanan mining district. Sulfide mineralization in the Ab-Bid deposit formed in Middle Triassic carbonate rocks and contains galena and sphalerite with minor pyrite, chalcopyrite, chalcocite, and barite. Silicification and dolomitization are the main wall-rock alteration styles. Structural and textural observations indicate that the mineralization occurs as fault fills with coarse-textured, brecciated, and replacement sulfides deposited in a bookshelf structure. The Ab-Bid ore minerals precipitated from high temperature (≈180–200 °C) basinal brines within the dolomitized and silicified carbonates. The sulfur isotope values of ore sulfides suggest a predominant thermochemical sulfate reduction (TSR) process, and the sulfur source was probably Triassic-Jurassic seawater sulfate. Given the current evidence, mineralization at Ab-Bid resulted from focusing of heated, over-pressurized brines of modified basinal origin into an active fault system. The association of the sulfide mineralization with intensely altered wall rock represents a typical example of such features in the Mississippi Valley-type (MVT) metallogenic domain of the TPMB. According to the structural data, the critical ore control is a bookshelf structure having mineralized dextral strike-slip faults in the northern part of the Ab-Bid reverse fault, which seems to be part of a sinistral brittle shear zone. Structural relationships also indicate that the strata-bound, fault-controlled Ab-Bid deposit was formed after the Middle Jurassic, and its formation may be related to compressive and deformation stages of the Mid-Cimmerian in the Middle Jurassic to Laramide orogenic cycle in the Late Cretaceous-Tertiary.

Keywords: Tabas-Posht e Badam metallogenic belt; Mississippi Valley-type; sulfide mineralization; non-sulfide mineralization; bookshelf structure; sinistral brittle shear zone

1. Introduction

Carbonate-hosted (CH) Zn-Pb deposits are widespread and share a broad spectrum of characteristics [1]. More than 350 CH Zn-Pb (±Ba±Cu±F) deposits are presently known in Iran (Figure 1a), including some world-class ore deposits such as Mehdiabad and Irankuh [2]. Recent contributions have established close temporal links between deposits

formation and regional geotectonic evolution of the Tethys oceans in Iran [3–6]. There is no precise information about the age of most of these deposits. However, their host rocks range from Cambrian to Tertiary [2–4], and mineralizations range from sub-seafloor replacement CH Zn-Pb Irish type to Mississippi valley-type (MVT). The most important metallogenic belts for these mineralizations are the Central Alborz, Tabas-Posht e Badam (TPMB), Malayer-Esfahan, and Yazd-Anarak (Figure 1a). Rajabi et al. [4] reviewed the metallogeny of CH Zn-Pb and F-rich deposits in the Tabas-Posht e Badam (TPMB, Figure 2) and Central Alborz metallogenic belts in the Iranian Plateau, and introduced the Permian–Triassic-hosted MVT ore province north of this Plateau.

The Kuhbanan-Behabad district is part of the TPMB, and is an extending southern part of this belt through the Central Iranian Microcontinent (Figure 2). In this district, Devonian to Late Cretaceous carbonate rocks host about 40 Zn-Pb (±Ba±F) MVT deposits, with about seven Mt Zn-Pb-Ba (±Cu) ores of exploited and known reserves. The principal producing mines hosted in the Shotory dolomites (Middle Triassic) of the Behabad area include Tarz, Gujer, Tajkuh, and Gijarkuh (Gicherkuh), which comprise non-sulfide and sulfide ores. Exciting areas of exploration are also located in the southeastern part of the district in the Kuhbanan area, including the Khorand, Dokuheh, Reyhan, Kand, and Ab-Bid deposits (Figure 2). The Ab-Bid deposit, hosted in Triassic carbonate rocks [2], is the subject of this paper. This deposit is located approximately 50 km south of Ravar and 25 km northwest of Kerman. The principal ore mineralizations of the Ab-Bid area are the Old Mine, New Mine, and Tunnel Messi (Figure 3). All of these mineralizations consist of strata-bound Zn-Pb (±Cu) non-sulfide and sulfide concentrations [7] that contain up to 1 Mt (pre-mining) of ore, averaging ~7% Zn + Pb. Its current remaining ore reserve is less than 0.4 Mt ore. The Ab-Bid mine produced ore from 1965 to 1977, before closing in 1977. The first geological studies in the Ab-Bid area were performed in 1963. The Hadid Bonyan Mining Company began to explore the deposit in 2013 by following old mining. Small adits, tunnels, and a dump at the eastern part of the Ab-Bid Mountain (Figure 3a) provide tangible evidence of historical mining activities. The geology and mineralogy of the Ab-Bid deposit were studied by Rajabi and Yarmohammadi [7,8]. In this contribution, we present geological, structural, and mineralogical data, and S-isotope signatures to constrain a genetic model for the carbonate-hosted Ab-Bid Zn-Pb (±Cu) deposit.

2. Geological Setting

The study area is located at the central part of the Central Iranian Microcontinent (Figure 1a), a crustal domain composed of three major structural zones, from E to W [9]: the Lut, Tabas, and Yazd blocks (Figure 1a,b), and the boundaries are defined by regional-scale faults (Figure 1a). In addition, there is the Posht-e-Badam Block [9], a fault-bound, variably deformed, and metamorphosed complex of supracrustal rocks that separates the Tabas and Yazd blocks (Figure 1). The Tabas Block is bounded by the Kuhbanan- Kalmard fault to the west and the Nayband fault to the east.

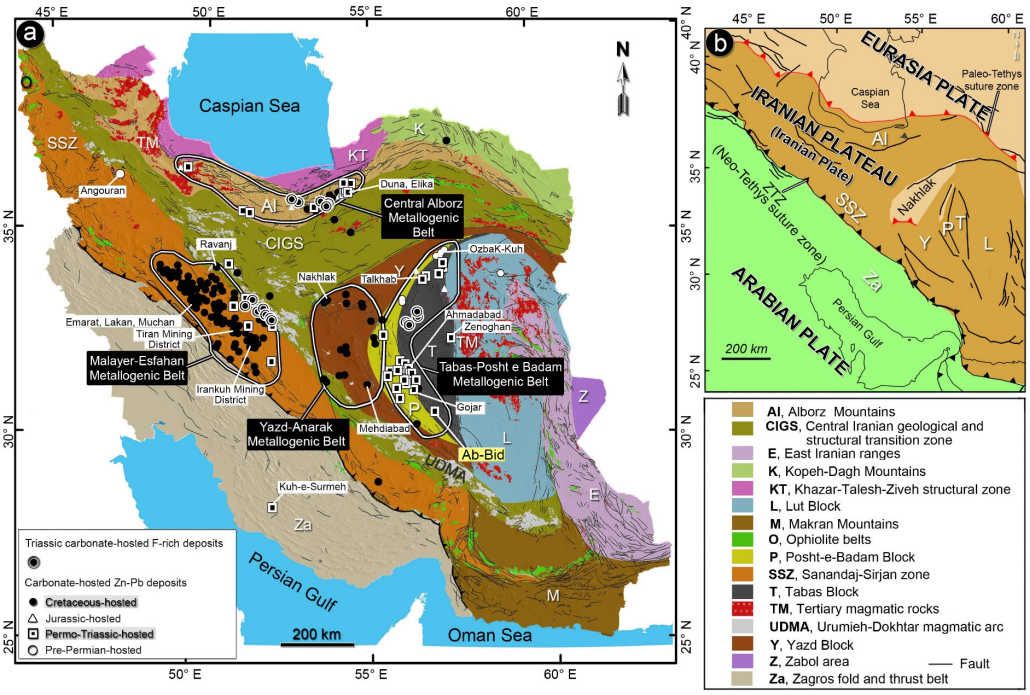

Figure 1. (**a**) Simplified tectonic map of Iran [5,10] and distribution map of carbonate-hosted (CH) Zn-Pb and F-rich deposits according to the age of host rocks in the Central Alborz, Tabas-Posht e Badam, Malayer-Esfahan, and Yazd-Anarak metallogenic belts [3,4]. Those in Permo-Triassic rocks include MVT deposits, but the Cretaceous-hosted deposits include Early Cretaceous Irish-type Zn–Pb and some MVT deposits [2]. (**b**) Simplified terrane map of the western Tethysides [5]. Note the location of the Iranian Plateau between the Arabian and Eurasia (Turan) plates.

The Central Iranian Microcontinent, together with the Sanandaj-Sirjan zone and the Alborz Mountains, form the Iranian Plateau, which occupies a structural key position in the Middle Eastern Tethysides (Figure 1b). The Iranian Plateau, which coincides with the Cimmerian terranes of Iran (Figure 1b), is located along the Tethyan sutures between Eurasia (Variscan domain) and the Arabian plates, and records the closure of at least two oceans, the Paleo-Tethys in the Mesozoic and the Neo-Tethys in the Cenozoic. The geology, and especially the tectonic evolution of the Iranian Plateau, are deeply influenced by the development and evolution of these two main Tethyan phases.

In the Early Silurian, the opening of the Paleo-Tethys detached the Turan region from Gondwana [11]. During the Permian and Triassic, the northern margin of the Iranian Plateau became a passive continental margin with extensive carbonate platforms [12]. The most important rifting phase in the south of the Iranian Plateau started during the Middle to Late Permian, when this continental block broke away from Gondwana. As a consequence, the Neo-Tethys Ocean opened, but an N-dipping subduction system developed along the Paleo-Tethys margin in the north of the Iranian Plateau [11,13], causing the closure of the Paleo-Tethys Ocean in the Late Triassic by subduction beneath the Eurasian plate margin (see the Paleo-Tethys suture in Figure 1b; [14,15]). From the Early Jurassic to the Eocene, the evolution of the present Central Iranian Microcontinent was directed by a sequence of back-arc extensional and compressional cycles that were controlled by the north-dipping subduction zone of the Neo-Tethys [15,16]. The collision of the Arabian Plate with the Iranian Plateau is inferred to have been initiated in the Late Eocene [17]. Detrital zircon ages [18] suggest this collision occurred between the middle Eocene and the Late Oligocene.

The Ab-Bid Pb-Zn (±Cu) deposit is located in the southern part of the Tabas Block (Figure 2), which is part of the TPMB. A geological map of this region is shown in Figure

3. All rock units in the district predominantly trend NW–SE, parallel to the Kuhbanan suture zone, southwest of the Tabas Block. The oldest units cropping out in the southwest are Early Cambrian red sandstone and conglomerate (Lalun or Dahu Formation), separated by a strike-slip fault zone from the Triassic and Jurassic rocks (Figure 3). Triassic limestones and dolomites (TR_{Sh}^{l}) host the bulk of the Pb-Zn (±Cu) mineralization at the Ab-Bid deposit, which is separated from other units by reverse-strike slip faults in the south. Moreover, in the northeastern boundary, the host unit is unconformably covered by the Late Triassic conglomerates, sandstones, and shales (TR_{N}^{csh}). This boundary is also indicated with small NW–SE trending faults in some parts.

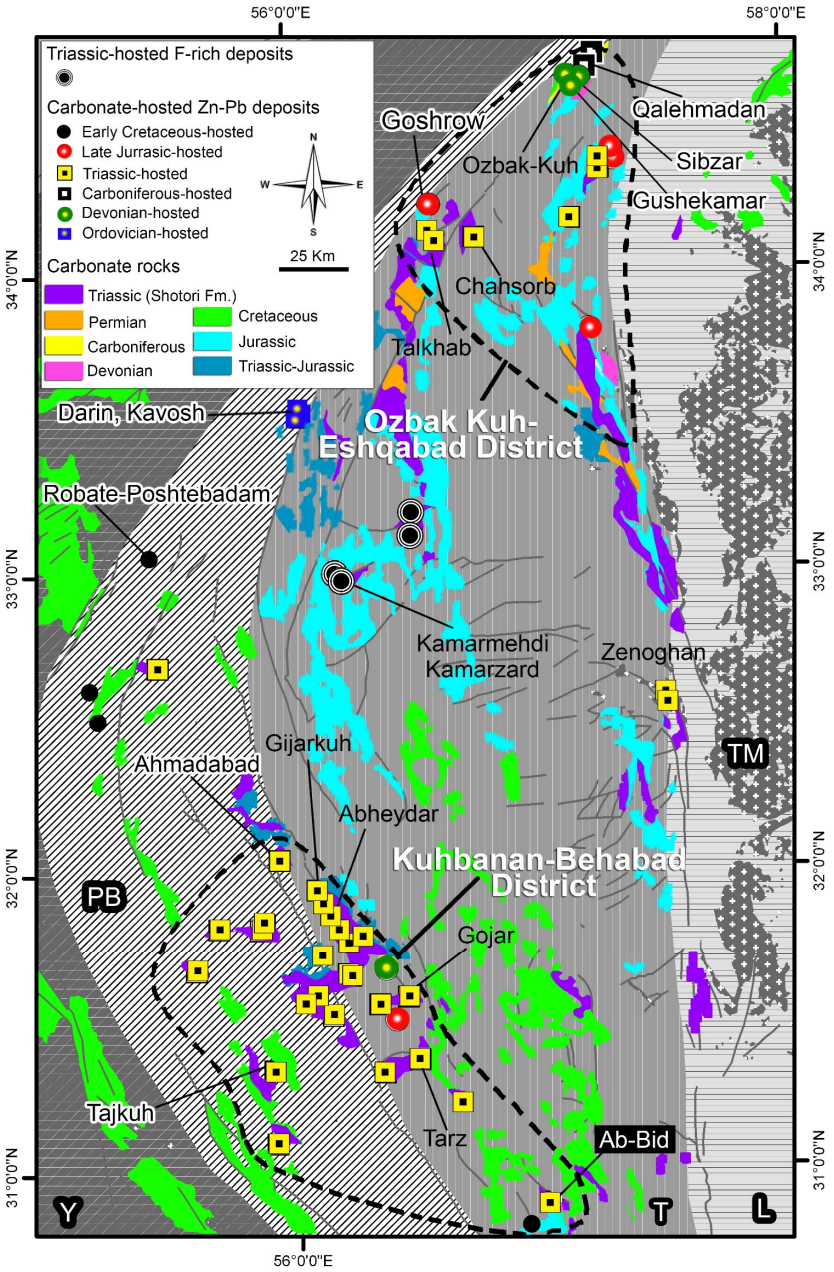

Figure 2. Distribution map of carbonate-hosted MVT and F-rich deposits in the Tabas-Posht e Badam metallogenic belt. Note the host rock age of MVT deposits (modified after [4]). Key: L, Lut Block; PB, Posht-e-Badam Block; T, Tabas Block; TM, Tertiary magmatic rocks; Y, Yazd Block.

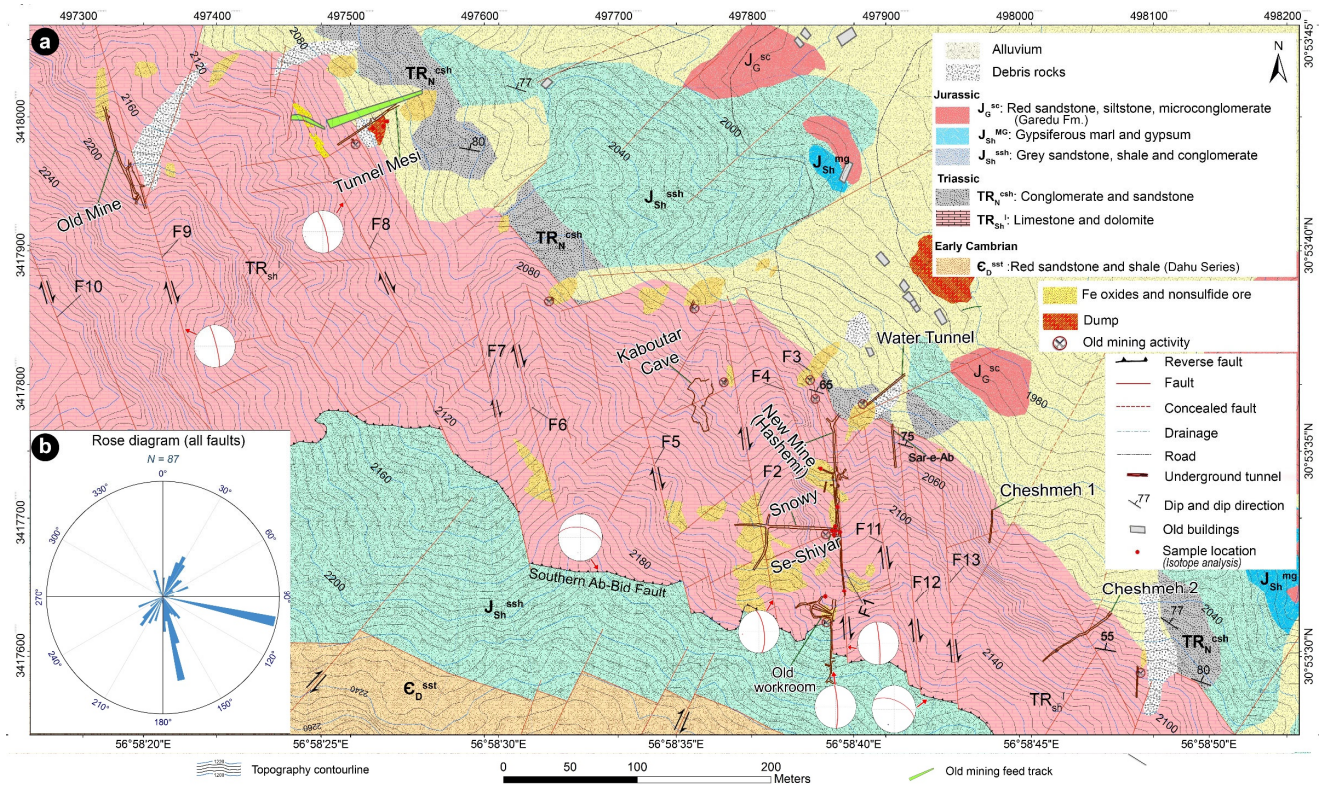

Figure 3. Geological map of the Ab-Bid deposit (**a**, modified after [7]) and direction of faults in this area (**b**). Stereographic projections (in (**a**)) show the orientations of major faults in the area.

The Early Jurassic rock unit (J_{Sh}^{ssh}) is composed of dark grey sandstone, shale, and a conglomerate of the Semshak series. This unit is overlain by gypsiferous marl and gypsum of the J_{Sh}^{mg} unit (Figure 3), and by the Upper Jurassic plant fossil-bearing red sandstone, shale, and microconglomerate of the Garedu (J_G^{sc}) Formation. The faults in this area are categorized into two different systems. The first system is a group of NW–SE-trending strike-slip and reverse faults that dominate in the mine area (Figure 3), and the mineralization is related to these faults. The second includes a set of NE–SW trending strike-slip faults with slight displacement.

3. Sampling and Methods

Representative samples of all mineralization styles and host rocks were collected from underground tunnels and adits within the Ab-Bid deposit. Mineralogical, textural, and paragenetic analyses were performed with the usage of reflected and transmitted light microscopy and scanning electron microscopy (SEM) at the University of Tehran, Iran. Thirteen sulfide samples from different ores of the Ab-Bid deposit were analyzed for sulfur stable isotope compositions.

Sulfide minerals were selected and separated mechanically (by crushing and hand-picking) after examining thin-polished sections to determine the primary mineralogy and purity of the areas to be sampled. Most samples were coarse enough to ensure >98% purity for the mineral separates. Sulfur isotopes were analyzed using a Delta C Finnigan MAT continuous-flow isotope-ratio mass spectrometer with an elemental analyzer. The isotopic analyses were carried out at the Centres Científics i Tecnològics of the Universitat de Barcelona, Spain. Results are reported in the conventional delta notation ($\delta^{34}S$) as per mil deviations from the V-CDT (Vienna Canyon Diablo Troilite) standard. The analytical precision is within ±0.1‰ (1σ).

4. Mineralization General Characteristics and Paragenesis

4.1. Hydrothermal Ore Mineralization

At the Ab-Bid deposit, the sulfide ores primarily occur in sheeted-like parallel veins, hosted by Triassic grey to light-brown limestone and dolomite (Figures 3 and 4), and are generally more developed in the New Mine (Figures 4–6). In the southeastern part of the deposit (New Mine), the veins are steep (85° NE), and their typical strike is N 352°, and are as long as 50 to 150 m and as thick as 0.5 to 3 m (Figures 4–7).

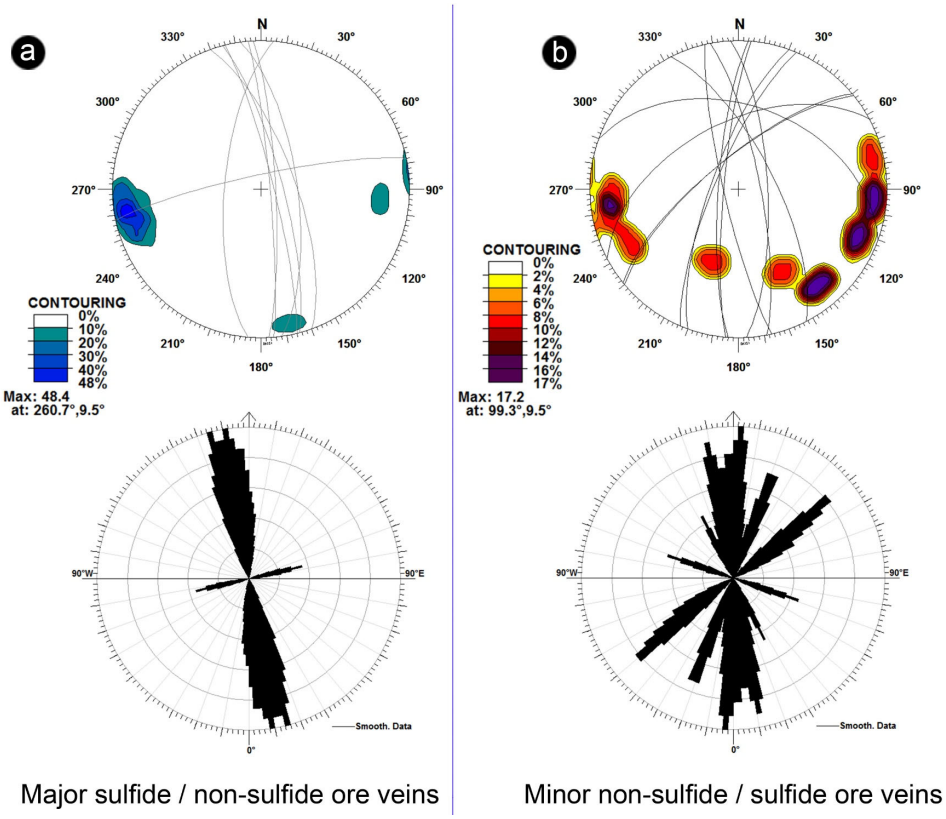

Figure 4. Stereographic projections and rose diagrams of the structural measurements of the major (**a**) and minor (**b**) ore veins in the Ab-Bid deposit. The lengths of the high-grade major ore veins are between 40 and 150 m, but those of the minor low-grade ore veins are less than 15 (1 to 15) m.

The strike-slip faults in domino structures are the main ore-controlling structure in the Ab-Bid deposit. The major ore veins can be divided into the lateral brecciated-veinlets ore zone (LOZ) and the central sulfide-rich ore zone (COZ) in this deposit (Figure 8). The LOZ, observed on both sides of the main ore veins (fault zone), is extended 1 to 3 m wide and is graded into unbroken carbonate rocks. This zone includes very low-grade sulfide mineralization and is characterized by dolomitized and silicified limestone with small sulfide-bearing dolomite-quartz veins and veinlets, disseminated and replacement sulfides, brecciated clasts, and a series of barren joints. On the microscopic scale, the brecciated clasts are intensely fractured and cut by microfractures infilled with Fe-dolomite, quartz, pyrite, and galena.

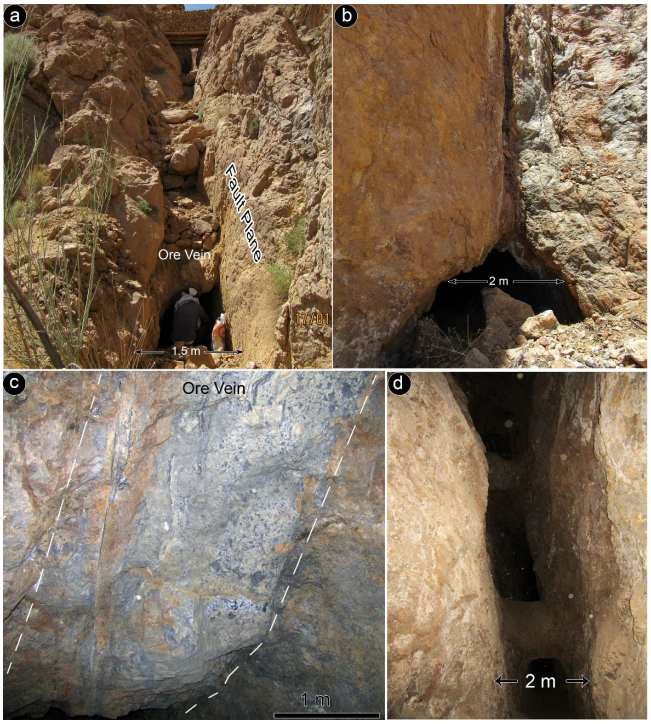

Figure 5. The outcrop of sulfide ore veins in extensional strike-slip faults on the surface (**a**,**b**) and underground tunnels (**c**,**d**).

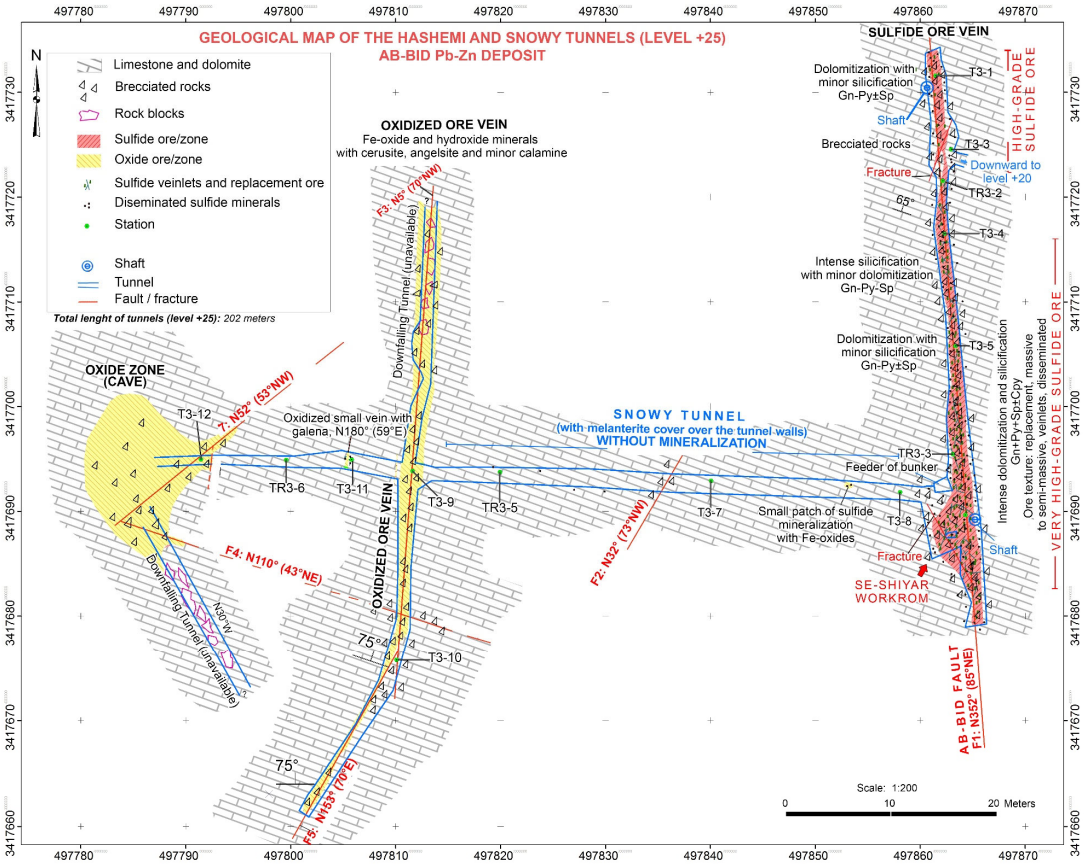

Figure 6. Geological map of the New Mine (Hashemi) and Snowy tunnels, +25 mining level [8].

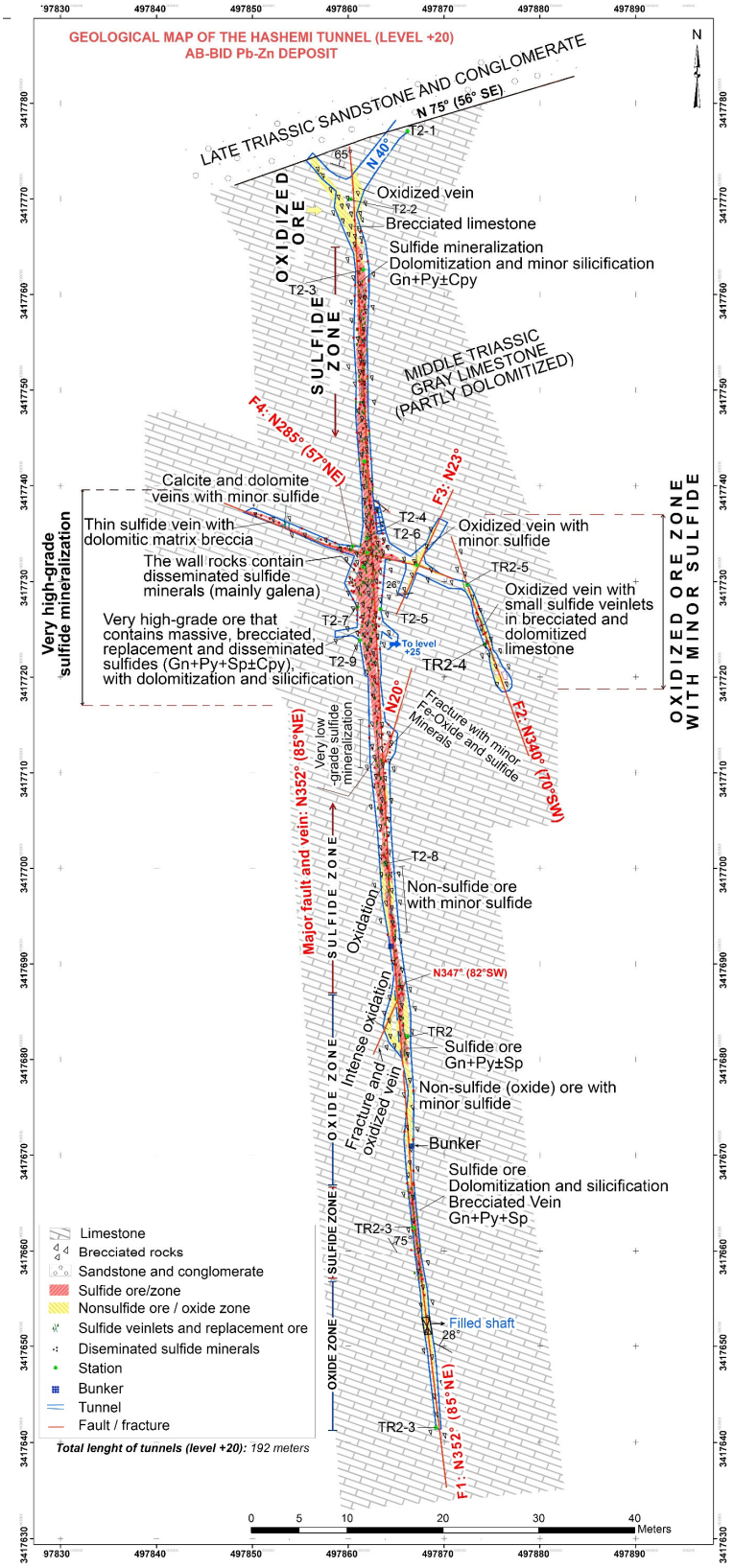

Figure 7. Geological map of the New Mine (Hashemi) tunnel, +20 mining level [8].

The central ore zone (COZ) is restricted to the core of the fault zones and ore veins. It consists of rounded centimeter-sized clasts in a hydrothermal dolomitic matrix with sulfide-rich mineralization and silicified patches (Figure 8). This ore zone at the Ab-Bid deposit has simple mineralogy. The main gangue minerals are dolomite, calcite, quartz, and subordinated barite, and the ore assemblage consists of galena, sphalerite, and pyrite, with minor chalcopyrite, chalcocite, and covellite (Figures 9 and 10). Sulfides occur mainly as veinlets, replacements, open space-filling, or cement in the limestone breccia (Figures 9 and 10). Galena is the main sulfide mineral in veins. The amount of chalcopyrite and chalcocite is higher in the northwestern veins of the deposit (Tunnel Messi), whereas galena and sphalerite are predominant in the southeastern veins. Moreover, pyrite increases upwards in these veins. Barite is rarely found in sulfide veins, associated with ferrous dolomite, and often occurs as small lenses with iron oxides in the central part of the deposit (Figure 9i), adjacent to the main mineralization veins. Galena occurs mainly as open space-filling matrix between breccia pieces and small veinlets, and also replaces Fe-dolomite and pyrite (Figure 10). Sphalerite has mainly replaced the previous sulfides, including galena and pyrite (Figure 10b–f). Chalcopyrite occurs in small veinlets and has been partly replaced by galena and sphalerite (Figure 10a–c).

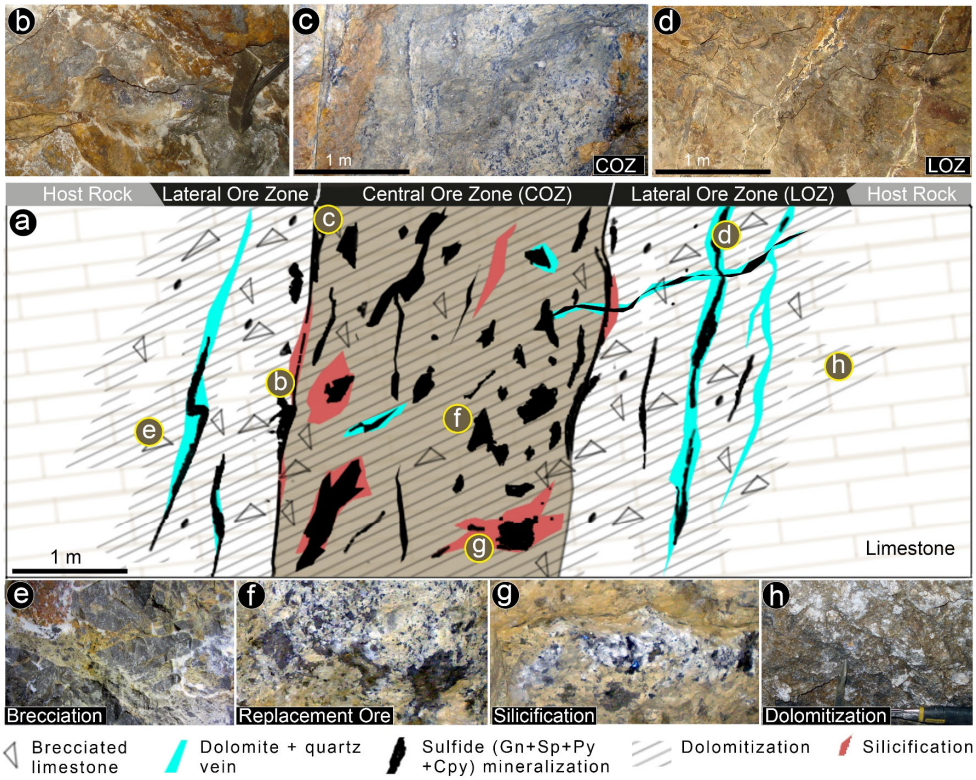

Figure 8. (**a**) A schematic structure of the central ore zone (COZ) and lateral ore zone (LOZ) in sulfide ore veins of the Ab-Bid deposit, showing different hydrothermal alterations and main ore textures. (**b**) Replacement of sulfides in wall-rock; (**c**) The central ore zone; (**d**) Sulfide-bearing veins and veinlets in the lateral ore zone (LOZ); (**e**) Brecciated limestone with hydrothermal dolomitization; (**f**) Replacement sulfide ore in the COZ; (**g**) Silicified patches with sulfide mineralization in the COZ, (**h**) Intense hydrothermal dolomitization in the LOZ.

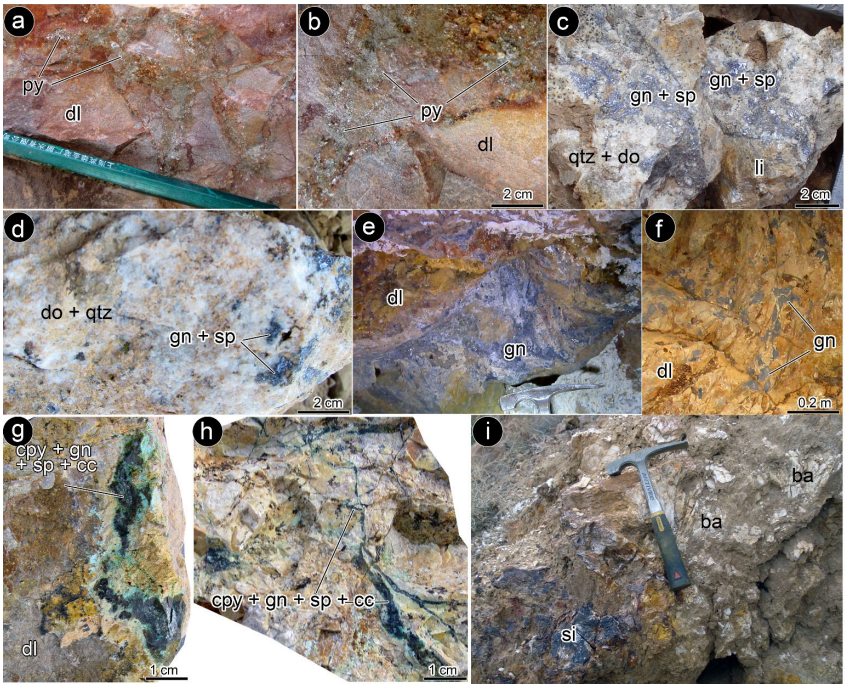

Figure 9. Hand specimen (**a**–**e**,**g**,**h**) and outcrop (**f**,**i**) photographs of sulfide and barite mineralization, Ab-Bid deposit. (**a**,**b**) Sparry dolomite, and pyrite (py) filling fractures within crackle breccia. (**c**–**f**) Replacement of hydrothermal dolomite (do), quartz (qtz), sphalerite (sp), and galena (gn) in dolomitic limestone (dl). (**g**,**h**) Chalcopyrite (cpy), galena, sphalerite, and chalcocite (cc) filling fractures within crackle breccia of dolomitized limestone (dl). (**i**) Massive barite (ba) mineralization in silicified (si) limestone.

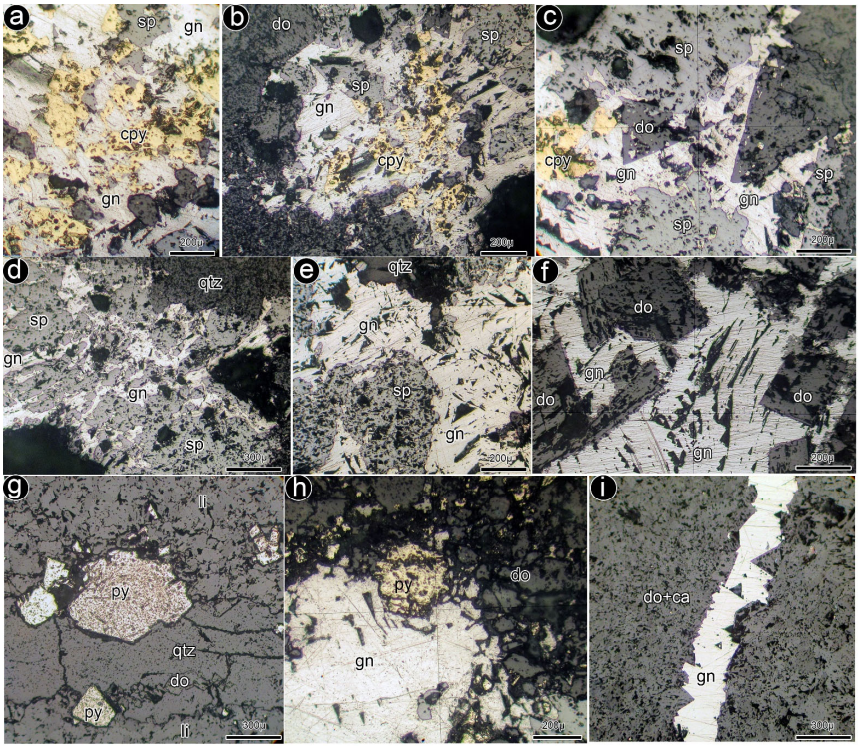

Figure 10. Microscopic photographs of complex replacement textures between sulfide minerals in replacement sulfide mineralization and dolomitized limestone. (**a**–**f**) Replacement of hydrothermal

dolomite and chalcopyrite with galena and sphalerite. In addition, galena was replaced with sphalerite. (**g**) Quartz (qtz) and dolomite (do) veins, associated with coarse-grained pyrite (py). (**h**) Replacement of pyrite with galena. (**i**) Galena veinlet in dolomite and calcite matrix.

Hydrothermal alteration in the Ab-Bid deposit mainly consists of dolomitization, silicification, host-rock dissolution, and brecciation in sulfide ore veins and the lateral ore zones (Figure 11). Hydrothermal dolomite occurs as a replacement of the host carbonates and as cement in brecciated rocks and open-space fill (Figure 11a–c). Calcite is common in some veins and is associated with dolomite. Another common alteration associated with LOZs in the Ab-Bid deposit is dissolution and hydrothermal brecciation of the carbonate host rocks. In addition, there are some silicified patches in both COZs and LOZs that contain high-grade sulfide ore (Figure 11d,e).

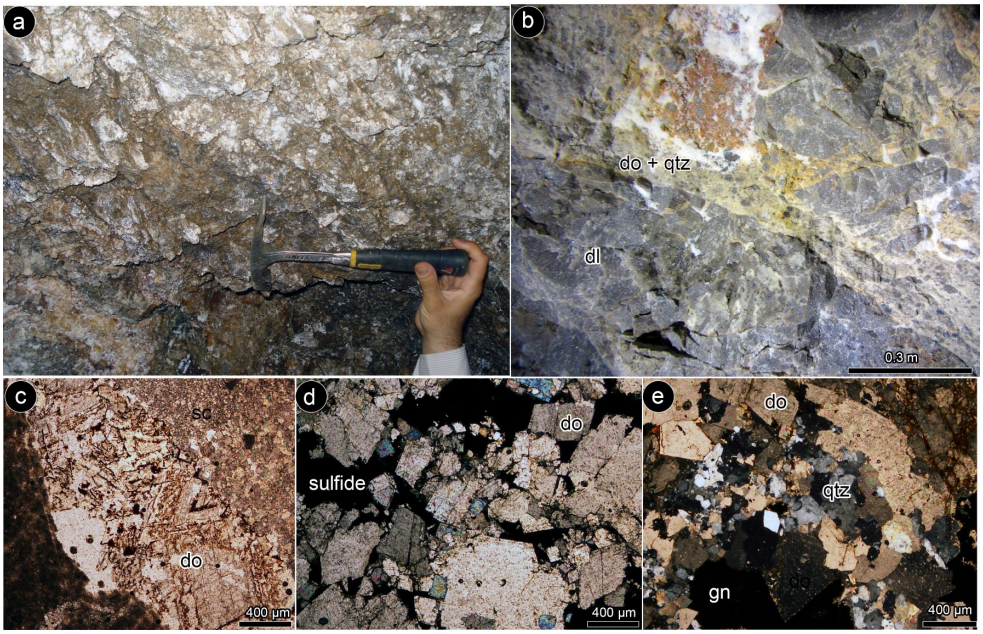

Figure 11. Outcrop (**a**,**b**) and microscopic ((**c**) ppl, (**d**) and (**e**) xpl) photographs of hydrothermal dolomite (dolomitization) and silicification in a brecciated host rock of the Ab-Bid deposit; do: dolomite, qtz: quartz, gn: galena, dl: dolomitized limestone.

4.2. Supergene Mineralization

At the Ab-Bid deposit, the western vein of New Mine and the near-surface parts of other ore veins in New Mine, Old Mine, and Tunnel Messi are exposed, completely oxidized, non-sulfide ores (Figures 6 and 12).

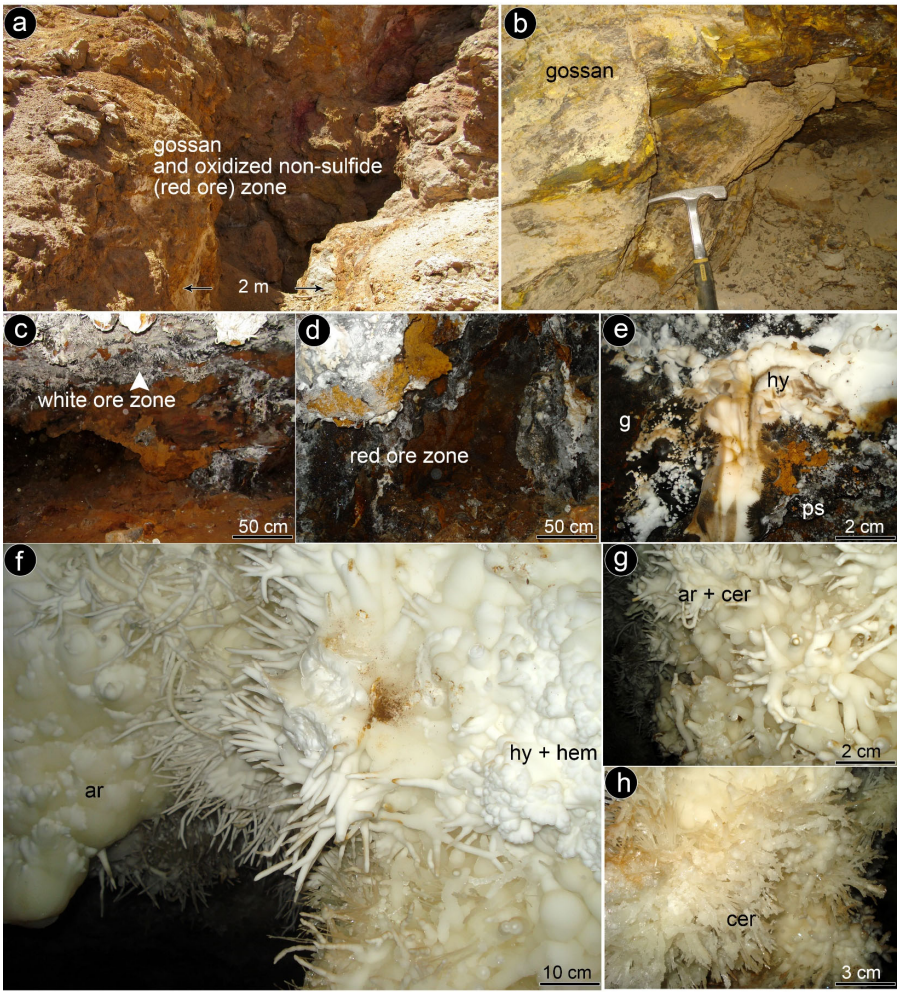

Figure 12. General view of the oxidized and supergene non-sulfide mineralization in the Ab-Bid deposit. (**a**,**b**) Gossan and oxidized non-sulfide (red ore) zone outcrops on the ground and underground caves. (**c**–**e**) Outcrop photographs of the red ore and white ore zones in underground tunnels and cavities. (**f**–**h**) Radial and euhedral cerussite (cer), aragonite (ar), hydrozincite (hy), and hemimorphite (hem) growing on the cavity walls and cave; pe: psilomelane.

The non-sulfide ore is generally controlled by the structures and is more developed at the junction of faults and joints (Figures 6 and 12a). The oxide mineralization in the upper parts of ore veins is more intense due to the presence of higher content of pyrite (Figures 9a,b and 12a,b). Gossan-like oxidized (or weathered) parts of the ores occurred not only at the surface of the primary sulfide veins, but also developed the infill of deeper fault-controlled cavities of ore veins in the host carbonates (Figure 12a–d). Oxidation of sulfides in these veins generally extends from the surface to an average of 50 m in depth. The gossan part of the deposit contains iron and manganese oxide and hydroxide minerals, such as hematite, goethite, and psilomelane (Figure 12b,d,e).

The non-sulfide ore in yellow to red surface areas (red zone ore), and areas in white color (white zone ore), occur as filling-pores, boxwork oxides, crustiform, and stalactite structures in the karst cavities (Figure 12c–h). The non-sulfide ore is rich in lead in the upper parts, and the zinc content increases in the middle to lower parts of the veins. Major non-sulfide minerals include cerussite, anglesite, hemimorphite, smithsonite, and hydrozincite. By comparison, the white ore contains higher amounts of zinc and less lead and iron hydroxides, whereas the red ore is mainly composed of iron oxides and hydroxides along with cerussite. The red ore is predominant in the upper parts of the main veins,

but the white ore shows little development in the karst sections and the middle part of the ore vein in New Mine.

5. Sulfur Isotopes

Sulfur isotopes were analyzed in 10 samples of galena, three of sphalerite, and three of barite, from the New Mine veins of the Ab-Bid deposit (Table 1). The results were compared with the $\delta^{34}S$ values of other CH Zn-Pb deposits of Iran and are displayed in Figure 13.

Table 1. Sulfur isotope data for galena, sphalerite, and barite of the Ab-Bid deposit.

Sample	Mineral	$\delta^{34}S$	Sample	Mineral	$\delta^{34}S$
Ab-Gn 1	Galena	−1.6	Ab-Gn 2	Galena	−1.9
Ab-Gn 3	Galena	−2.1	Ab -Gn 10	Galena	−1.7
Ab-Gn 4	Galena	−1.0	Ab-Sp 1	Sphalerite	2.5
Ab-Gn 5	Galena	−1.0	Ab-Sp 2	Sphalerite	1.4
Ab -Gn 6	Galena	−1.0	Ab-Sp 3	Sphalerite	1.2
Ab -Gn 7	Galena	−1.9	Ab-Ba 1	Barite	18.2
Ab -Gn 8	Galena	−1.9	Ab-Ba 2	Barite	12.3
Ab -Gn 9	Galena	−2.1	A -Ba 3	Barite	15.7

The $\delta^{34}S$ values of sulfides from the Ab-Bid deposit show a relatively narrow range of variation, from −2.1 to +2.5‰, with an average of −0.8‰. Three barite samples from the western vein of the New Mine gave $\delta^{34}S$-enriched values, between +12.3 and +18.2‰.

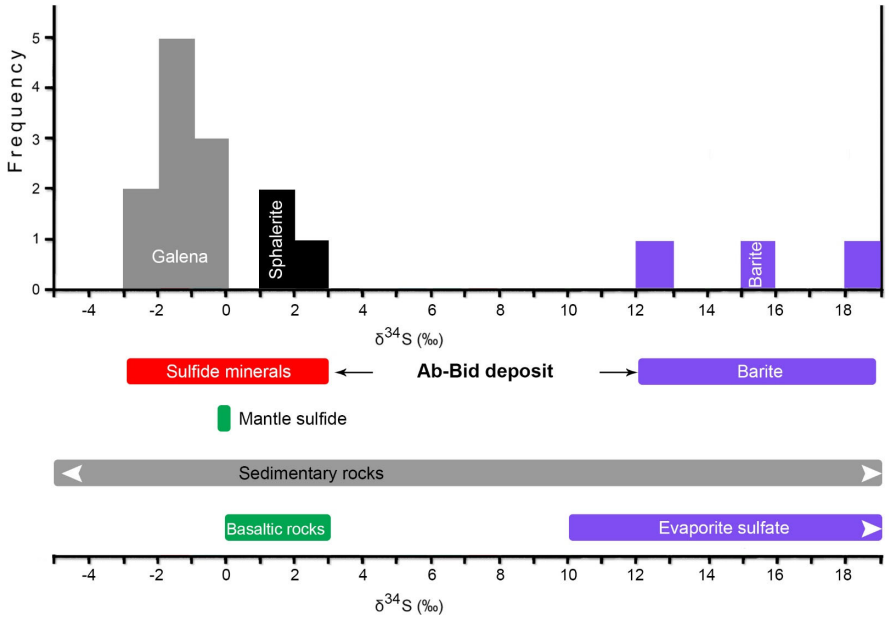

Figure 13. Histogram of $\delta^{34}S$ values for sulfides and barite from the Ab-Bid deposit in comparison with $\delta^{34}S$ values of evaporite sulfate, mantle sulfide, basaltic, and sedimentary rocks [19].

6. Discussion

6.1. Structural Controls on Mineralization

Although in most CH Pb-Zn deposits, the ore is localized in dilatancy zones associated with faults [20], at the Ab-Bid these structures are important ore controls of the mineralization, which occurs in NW–SE trending strike-slip faults (Figure 14).

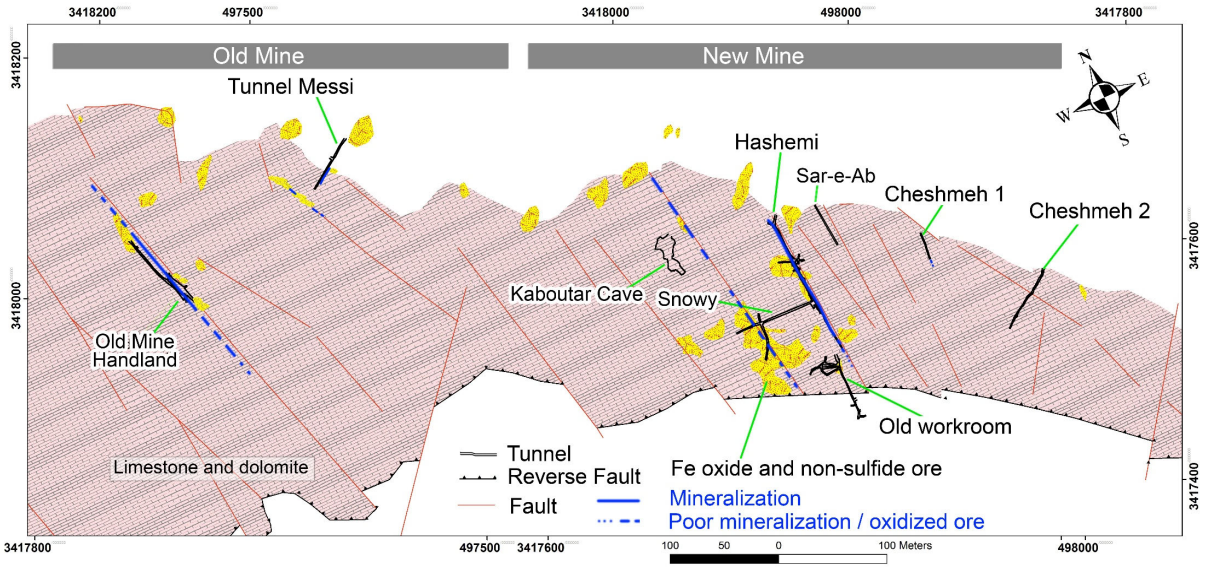

Figure 14. Simplified structural map of the host carbonate rocks and location of underground tunnels and adits, Ab-Bid deposit.

Except for the ore vein in the Tunnel Messi (N 50°), northwest of the Ab-Bid deposit, other sulfide veins studied in the New Mine of the deposit follow the NW–SE trend and vary from N 352° in the southeast of New Mine to N 340° in the northwest of Old Mine. Moreover, the mineralization of veins in the Ab-Bid deposit is limited to the host carbonate rocks and is cut by the southern Ab-Bid fault in the south.

The north and northeastern boundaries of the host carbonate are indicated by an unconformity between Middle Triassic carbonates and Late Triassic conglomerates and sandstones (Figure 3). This boundary also shows a strike-slip component, with a general trend of N 325° and dip of 20° SW in some parts, defining new movement in this boundary of the host carbonate rocks with the upper succession in the north and northeastern parts of the deposit. However, given the general trend of N 285°, the southern Ab-Bid fault is a reverse type that led the carbonate-hosted section to be thrust on the detrital sedimentary rocks of the Ab-Bid area (Figure 14).

The sulfide veins in the Ab-Bid deposit were formed along the faults with the NW-SE trend, representing their normal function with strike-slip extensional movements among the rock blocks of Triassic carbonates. The orientation of normal faults with right-handed strike-slip functions in relation to the southern Ab-Bid reverse fault represents a bookshelf tectonic structure in the carbonate rocks of the Ab-Bid area (Figure 15). These structures record a sinistral strike-slip brittle shearing in the Ab-Bid area, and the blocks of Triassic carbonate rocks were rotated counterclockwise within this shear zone (Figure 15a,b). Furthermore, this rotation is accompanied by the creation of normal faults with the dextral strike-slip component and the formation of dilatational expansion spaces among faults in Middle Triassic carbonates.

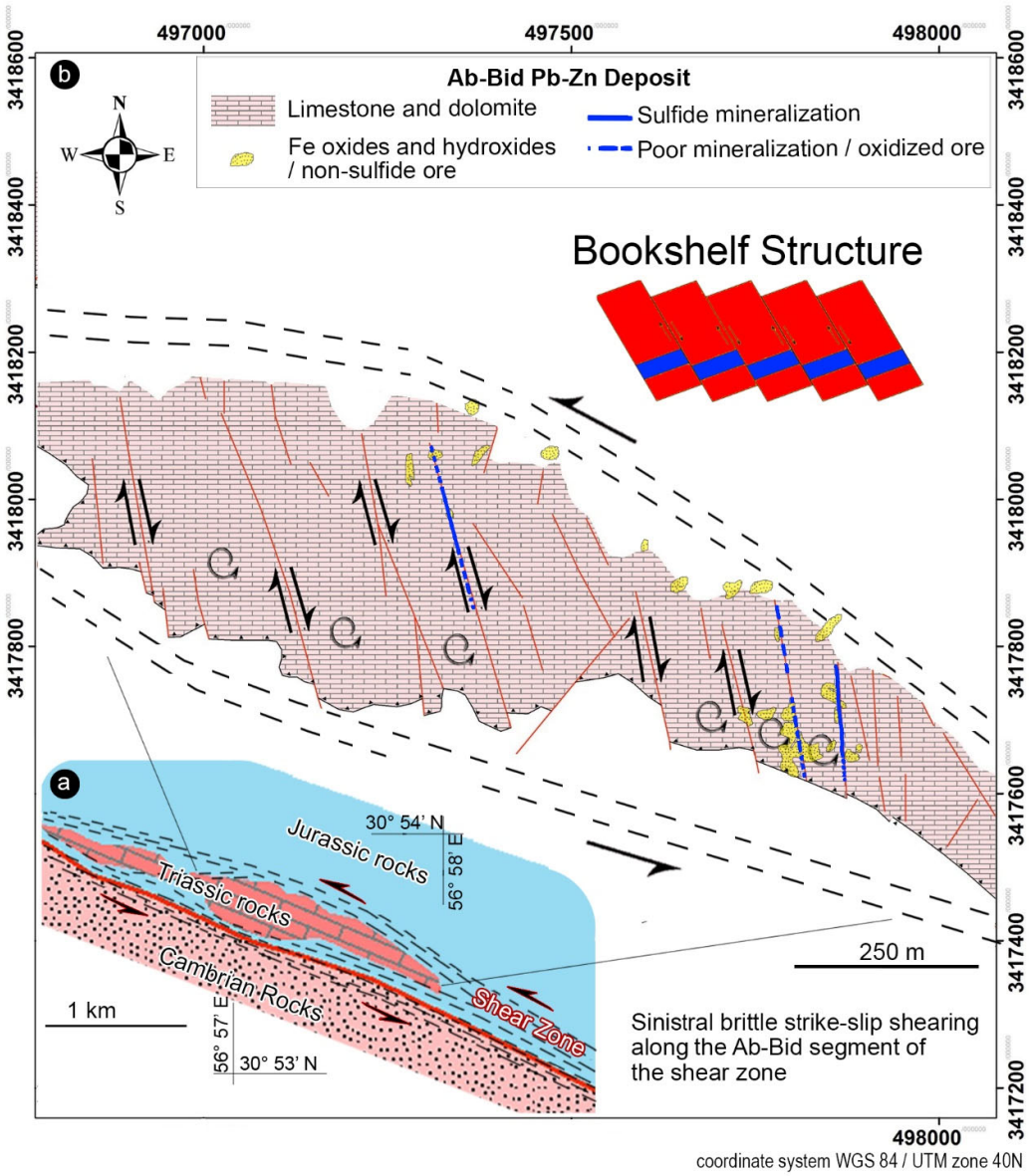

Figure 15. (**a**) A sinistral brittle strike-slip shearing along the Ab-Bid segment of the shear zone (dotted lines). (**b**) Illustration of the bookshelf structure in carbonate host rocks of the Ab-Bid deposit and structural control of sulfide mineralization.

From the mechanical point of view, the bookshelf structure is formed by the rotation of rock blocks and predominantly parallel faults with a similar mechanism in response to an imposed crustal extension or shortening movements. In the Ab-Bid area, the fault movements of the region were affected by a large Kuhbanan seam in the east of Tabas block, so that most of the faults in the region are formed in a similar direction to this seam. A strike-slip fault puts the Cambrian and Precambrian rock sections in contact with the Triassic and Jurassic section (Figure 15). The movement of these two rock platforms during the compression phases, and the sinistral movement of the Southern Ab-Bid fault in a shear zone, have led to the formation of a bookshelf structure in Triassic carbonates. These movements have also provided suitable tensile spaces for mineralization.

6.2. Sulfur Origin

Sulfide minerals in almost all CH Pb-Zn deposits show wide ranges of $\delta^{34}S$ (Figure 16), with values from negative (>−25‰) to positive (<+35‰) [20]. However, the sulfide minerals in the Ab-Bid Pb-Zn (±Cu) deposit show a relatively narrow range of $\delta^{34}S$ values, from −2.1‰ to +2.5‰, with an average of −0.8‰ (Figure 16). Although this narrow range may be caused by the limited number of analyzed samples of sulfides, the values of $\delta^{34}S$ also may suggest a uniform isotopic composition of the source and uniform conditions governing the isotopic fractionation between sulfur species in the ore-forming fluids during mineralization.

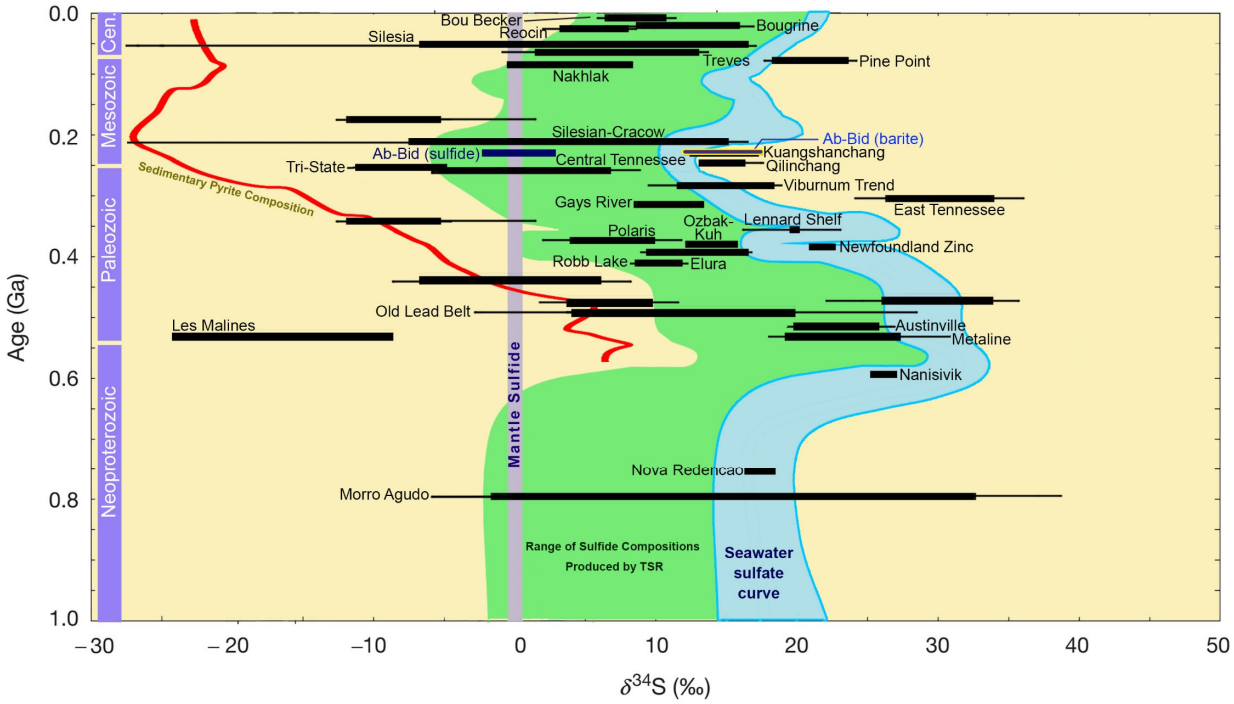

Figure 16. Diagram illustrating the range of $\delta^{34}S$ values in sulfides and barite of the Ab-Bid deposit in comparison with the range and median $\delta^{34}S$ values of sulfides in a selection of orogenic-related MVT deposits (data from [2,3,20–25]), seawater sulfate curve [26], mantle sulfide, and mean sedimentary pyrite composition (red line) as produced by bacterial sulfate reduction (BSR) [22]. The green-shaded field indicates the likely range of sulfide compositions produced by thermochemical sulfate reduction (TSR) of seawater-derived sulfate at 150 °C [27]. Sulfur in most MVT deposits, in addition to the Ab-Bid deposit, is consistent with an origin from seawater sulfate, reduced by TSR.

Seawater sulfate is considered the predominant source of sulfur in CH Pb-Zn deposits [21]. However, a magmatic source can also be the ultimate source of sulfur that causes uniform sulfur isotopic compositions in sulfide mineralization [28]. These $\delta^{34}S$ data on sulfide minerals show a narrow distribution (average $\delta^{34}S$ value of sulfide = −0.8‰, Figure 13) similar to values of magmatic-hydrothermal deposits. However, the strongly positive $\delta^{34}S$ values of barite (+15.4‰ in average) are higher than the values of typical magmatic sulfur (0‰ ± 5‰, [28]), and refuse the magmatic source. In addition, the $\delta^{34}S$ values of barite and sulfides fall in the range of sedimentary rocks, and a marine sulfate source of sulfur is suggested (Figure 13).

The sulfur isotopic composition of Triassic seawater sulfate is between +11 and +20‰ [26,29]. The carbonate-host rock of the Ab-Bid deposit is thought to belong to the Triassic, and the $\delta^{34}S$ values of barite (Figure 16) in this deposit fall in the range of Triassic marine sulfate. Thermochemical and bacterial sulfate reduction (TSR and BSR, respectively) are the most relevant processes that modify sulfur isotopic composition from the seawater

sulfate in MVT deposits [21,22]. It should also be considered that the distribution of $\delta^{34}S$ values also depends on other factors such as sulfate reduction rate [30], sulfate concentration [31], temperature [32], the content of organic-rich matter in the sediments [33], and the rate of sulfate replacement with sulfides [34]. Bacterial sulfate reduction (BSR) or microbial sulfate reduction (MSR) occurs at temperatures of <110 °C [35,36] and results in a broad range of light isotopic (negative $\delta^{34}S$) values. Sulfur isotopic fractionation (Δ) of BSR ranges from −20 to −60‰ (Δ −40‰ on average) relative to the parent sulfate, which is why negative $\delta^{34}S$ values are usually produced. By comparison, thermochemical sulfate reduction (TSR) causes isotopic fractionation of $\delta^{34}S$ values by as much as −15‰ relative to the parent sulfate [37,38]. Furthermore, TSR is ineffective at T < 125 °C because of the slow reaction kinetics [39]. The calculations of temperature from sphalerite-galena sulfur isotope pairs using the fractionation equation by Ohmoto and Rye [28] yield 186 to 203 °C. TSR has been invoked as an important sulfate reduction process in MVT deposits [20]. It is likely that such a fractionation mechanism can explain the isotopic composition of sulfides in the Ab-Bid deposit. Indeed, in these veins, the $\delta^{34}S$ sulfide values are not consistent with BSR, and fluid temperatures are too high for BSR or MSR to occur. Above 125 °C, sulfate can be reduced to sulfide through TSR (Figure 16), where smaller fractionations between the sulfate and sulfide minerals occur under higher temperatures. The Ab-Bid deposit in Triassic carbonate rocks is located adjacent to the Late Jurassic Nayband Formation, deposited in a foreland basin. This formation contains preserved organic matter such as coal beds rich in plant fossils. Therefore, we suggest that sulfate was most likely transported in sulfate-bearing fluids and reacted with the organic matter in the Nayband Formation. Above 125 °C and in the presence of organic matter as a reducing agent, sulfate can be reduced to sulfide through TSR (Figure 16) at the mineralization site.

6.3. Ore Deposit Type and Ore Genesis

The Ab-Bid Pb-Zn (±Cu) deposit is hosted mainly by Middle Triassic carbonates, and the dominant sulfide minerals are galena, sphalerite, pyrite, and chalcopyrite, associated with hydrothermal barite, dolomite, calcite, and quartz. According to the structural data in this deposit, the critical ore control is a bookshelf structure with mineralized dextral strike-slip faults in the northern part of the Ab-Bid reverse fault, which seems to be part of a sinistral brittle shear zone. The mineralization is strata-bound and epigenetic, as shown by veins, and brecciated and open-space-fill ore styles. Hydrothermal alteration consists mainly of dolomitization and silicification, associated with host-rock dissolution and brecciation; thus, it roughly fits with an MVT deposit model. Nevertheless, the Ab-Bid Pb-Zn (±Cu) deposit contrasts with typical MVT deposits by the presence of Cu, lack of dissolution–collapse breccias, and dominance of open-space filling relative to replacement of carbonate rocks.

Rajabi et al. [3,4] proposed that the Main-Cimmerian (Upper Triassic) and Laramide (Late Cretaceous-Tertiary) orogenic collisions led to the development of discordant, strata-bound MVT deposits in different Zn-Pb metallogenic belts of Iran around the Paleo-Tethys and Neo-Tethys suture zones. Leach et al. [20,21,23] proposed that Devonian to Lower Triassic times were an important interval for the formation of MVT deposits worldwide, and the development of many foreland basins coincided with intense orogenic tectonic events. MVT deposits are formed from large hydrothermal systems in foreland basins, so that the fluid drive may be diagenesis and compaction within the source basin or by orogenic tectonic processes [20]. Rajabi et al. [4] proposed that the Main-Cimmerian orogenic events transformed the northern margin of the Iranian Plateau into a collisional foreland basin (Upper Triassic-Early Jurassic). This compression 'squeezed' fluid flow from the foreland basin towards the carbonate platforms (Elika and Shotori Formations) in Central Iran and formed MVT Zn–Pb (and F-rich Pb-Zn) mineralizations (Late-Triassic-Early Jurassic) in the Tabas-Posht e Badam metallogenic belt.

An Upper Triassic unconformity separates Middle Triassic carbonates (Elika and Shotori formations) from the Shemshak Group and the equivalent Nayband Formation in

Central Iran and Alborz region (see Figures 5 and 8 in Rajabi et al. [4]). The Upper Triassic–Middle Jurassic Shemshak Group, is commonly regarded as the Cimmerian foreland molasses [40], and most of the MVT deposits of Iran, as well as the Ab-Bid deposit, occur immediately below the Main-Cimmerian orogenic unconformity. This unconformity, along with the Mid-Cimmerian unconformity over the Shemshak Group, indicates the first major orogenic event related to the closure of the Paleo-Tethys ocean in the north of the Iranian Plateau. However, the age of the ore-related structures in the Ab-Bid deposit is still poorly constrained, but the ore-bearing faults in this area were formed after thrust movement along the southern Ab-Bid fault, and are younger than Early to Middle Jurassic foreland sediments. Therefore, the formation of ore-bearing faults may be related to compressive, and deformation stages of the Mid-Cimmerian in the Middle Jurassic to Laramide orogenic cycle started in the Upper Cretaceous-Tertiary.

In the Ab-Bid area, during the compressional and deformation events and releasing of mineralizing fluids from underlying foreland sediments (Shemshak and Magu groups), the ore fluids moved to the carbonate rocks of Shotori Formation (Middle Triassic). These fluids were trapped and concentrated into the fractured, brecciated, and dolomitized fault zones of the host carbonates. The Southern Ab-Bid reverse fault acted as a conduit and created permeability to provide suitable pathways for ore fluid migration to the carbonate host rocks.

The Ab-Bid ore minerals precipitated from relatively high temperature basinal brines (≈180–200 °C) within the dolomitized and silicified carbonates. The sulfur isotope values of ore sulfides suggest a predominant TSR process, and the sulfur source was probably Triassic-Jurassic seawater sulfate. Although we do not have lead isotope analyses, the lead source in the Ab-Bid deposit may be linked to the Triassic-Jurassic sandstone paleo-aquifers (foreland basin) in Central Iran. The sulfide ore precipitation was mostly the result of the interaction of ore fluid with the carbonate host rocks, decreasing temperature, increasing pH, and maybe a drop in oxygen fugacity, and therefore, an increase in reduced sulfur by TSR.

7. Conclusions and Implications for Mineral Exploration

This structural-geological study of the Ab-Bid Zn-Pb (±Cu) deposit provides a precise picture of the processes and structures that control the MVT mineralization in the Kuhbanan area, Tabas-Posht e Badam metallogenic belt during the Late Triassic to Jurassic. The previous models suggest that the MVT deposits in the TPMB are related to the Late Triassic Main-Cimmerian orogenic event, but structural relationships indicate that the strata-bound, fault-controlled Ab-Bid deposit was formed after the Middle Jurassic, and its formation may be related to compressive and deformation stages of the Mid-Cimmerian in the Middle Jurassic to Laramide orogenic cycle in the Late Cretaceous-Tertiary.

Based on the ore characteristics observed in the Ab-Bid MVT deposit, an exploration model for the discovery of Zn-Pb deposits in the region should consider the presence of structural controls, particularly the bookshelf/domino tectonic structure, dextral strike-slip faults with extensional movements that are related to reverse faults, and carbonate rocks/blocks trusted or reversed over foreland sediments (sandstone and shales with organic matter), as favorable factors for mineralization.

The presence of carbonate rocks that were thrust (or reversed) over the detrital organic material (coal, organic matter, or graphite) is an essential factor in the formation of MVT deposits in Central Iran. Organic matter-bearing foreland sediments can act as ore fluid sources and serve as a reducing agent in MVT ore deposits of the TPMB, and may be used as one factor in a prospective program. Finally, the essential component of the exploration model is the recognition of structures associated with domino movements related to a reverse or thrust fault in carbonate rocks as ore traps, which must be considered as a factor in prospective programs.

Author Contributions: Conceptualization, A.R., C.C. and P.A.; methodology, A.R. and P.A.; software, S.R.; validation, A.R., P.A. and C.C.; formal analysis, P.A.; investigation, A.R., A.Y., A.M. and C.C.; data curation, A.R., C.C. and P.A.; writing—original draft preparation, A.R. and P.M.; writing—review and editing, C.C., P.A. and S.S.; project administration, A.R. All authors have read and agreed to the published version of the manuscript.

Funding: This research received no external funding.

Acknowledgments: The Serveis Científico-Tècnics de la Universitat de Barcelona and the research grant 2009SGR-00444 of the Departament d'Universitats, Recerca I Societat de la Informació (Generalitat de Catalunya) supported sulfur isotope analyses. The authors thank Hadid Bonyan Mining Company (HMC) and Khaki for allowing access to the deposit and providing valuable support onsite through access underground exposures. The manuscript has benefited from helpful comments by three anonymous reviewers.

Conflicts of Interest: The authors declare no conflict of interest.

References

1. Sangster, D.F. Carbonate-hosted Lead-zinc Deposits: 75th Anniversary Volume. *Econ. Geol.* **1996**, *4*. https://doi.org/10.5382/SP.04.
2. Rajabi, A. *Metallogeny and Geology of Sediment-Hosted Zn-Pb Deposits of Iran*; University of Tehran Press: Tehran, Iran, 2022.
3. Rajabi, A.; Rastad, E.; Canet, C. Metallogeny of Cretaceous carbonate-hosted Zn–Pb deposits of Iran: Geotectonic setting and data integration for future mineral exploration. *Int. Geol. Rev.* **2012**, *54*, 1649–1672. https://doi.org/10.1080/00206814.2012.659110
4. Rajabi, A.; Rastad, E.; Canet, C. Metallogeny of Permian–Triassic carbonate-hosted Zn–Pb and F deposits of Iran: A review for future mineral exploration. *Aust. J. Earth Sci.* **2013**, *60*, 197–216. https://doi.org/10.1080/08120099.2012.754792
5. Rajabi, A.; Mahmoodi, P.; Rastad, E.; Niroomand, S.; Canet, C.; Alfonso, P.; Shabani, A.A.T.; Yarmohammadi, A. Comments on "Dehydration of hot oceanic slab at depth 30–50 km: Key to formation of Irankuh-Emarat Pb-Zn MVT belt, Central Iran" by Mohammad Hassan Karimpour and Martiya Sadeghi. *J. Geochem. Explor.* **2019**, *205*, 106346.
6. Karimpour, M.H.; Sadeghi, M. Dehydration of hot oceanic slab at depth 30–50 km: KEY to formation of Irankuh-Emarat PbZn MVT belt. Central Iran. *J. Geochem. Explor.* **2018**, *194*, 88–103.
7. Rajabi, A.; Yarmohammadi, A. Geologic Map (1:5000) and Report for the Ab-Bid Pb-Zn (Cu) Deposit, South of Ravar, Central Iran; Hadid Bonyan Mining Company: Esfahan, Iran, 2015.
8. Rajabi, A.; Yarmohammadi, A. Geologic Map of Underground Tunnels (1:200) and Report for the Ab-Bid Pb-Zn (Cu) Deposit, Central Iran; Hadid Bonyan Mining Company: Esfahan, Iran, 2016.
9. Alavi, M. *Tectonic Map of the Middle East; Scale 1:5000000*; Geological Survey of Iran: Tehran, Iran,1991.
10. Aghanabati, A. Major sedimentary and structural units of Iran (map). *Geosciences* **1998**, *7*, 29–30.
11. Golonka, J. Plate tectonic evolution of the southern margin of Eurasia in the Mesozoic and Cenozoic. *Tectonophysics* **2004**, *381*, 235–273.
12. Alavi, M. Tectonics of the Zagros orogenic belt of Iran: New data and interpretations. *Tectonophysics* **1994**, *229*, 211–238.
13. Ghasemi, A.; Talbot, C.J. A new tectonic scenario for the Sanandaj-Sirjan Zone (Iran). *J. Asian Earth Sci.* **2005**, *26*, 683–693.
14. Alavi, M. Tectonostratigraphic synthesis and structural style of the Alborz Mountains system in northern Iran. *J. Geodyn.* **1996**, *11*, 1–33.
15. Bagheri, S.; Stampfli, G.M. The Anarak, Jandaq and Posht-e-Badam metamorphic complexes in central Iran: New geological data, relationships and tectonic implications. *Tectonophysics* **2008**, *451*, 123–155.
16. Bagheri, S.; Gol, S.D. The eastern Iranian orocline. *Earth Sci. Rev.* **2020**, *210*, 103322.
17. Allen, M.B.; Armstrong, H.A. Arabia–Eurasia collision and the forcing of mid-Cenozoic global cooling. *Palaeogeogr. Palaeoclimatol. Palaeoecol.* **2008**, *265*, 52–58.
18. Horton, B.K.; Hassanzadeh, J.; Stockli, D.F.; Axen, G.J.; Gillis, R.J.; Guest, B.; Grove, M. Detrital zircon provenance of Neoproterozoic to Cenozoic deposits in Iran: Implications for chronostratigraphy and collisional tectonics. *Tectonophysics* **2008**, *451*, 97–122.
19. Hoefs, J. *Stable Isotope Geochemistry*; Springer: Berlin, Germany, 2015.
20. Leach, D.L.; Sangster, D.F.; Kelley, K.D.; Large, R.R.; Garven, G.; Allen, C.R.; Gutzmer, J.; Walters, S. Sediment-hosted lead-zinc deposits: A global perspective. *Econ. Geol.* **2005**, *100*, 561–607.
21. Leach, D.L.; Taylor, R.D.; Fey, D.L.; Diehl, S.F.; Saltus, R.W. A deposit model for Mississippi Valley-type lead-zinc ores. *Chapter A Miner. Depos. Models Resour. Assess. USGS Sci. Investig. Rep.* **2010**, 5070–A. https://doi.org/10.3133/sir20105070A.
22. Wilkinson, J.J. Sediment-Hosted Zinc-Lead Mineralization: Processes and Perspectives: Processes and Perspectives, 2nd ed.; Treatise on Geochemistry: London, UK, 2014; pp. 515–541.
23. Leach, D.L.; Bradley, D.; Lewchuk, M.T.; Symons, D.T.; Marsily, G.; Brannon, J. Mississippi Valley-type lead–zinc deposits through geological time: Implications from recent age-dating research. *Miner. Depos.* **2001**, *36*, 711–740.
24. Jazi, M.A.; Karimpour, M.H.; Shafaroudi, A.M. Nakhlak carbonate-hosted Pb (Ag) deposit, Isfahan province, Iran: A geological, mineralogical, geochemical, fluid inclusion, and sulfur isotope study. *Ore Geol. Rev.* **2017**, *80*, 27–47.

25. Ehya, F. The Paleozoic Ozbak-Kuh carbonate-hosted Pb-Zn deposit of East Central Iran: Isotope (C, O, S, Pb) geochemistry and ore genesis. *Mineral. Petrol.* **2014**, *108*, 123–136.
26. Bottrell, S.H.; Newton, R.J. Reconstruction of changes in global sulfur cycling from marine sulfate isotopes. *Earth Sci. Rev*. **2006**, *75*, 59–83.
27. Kiyosu, Y.; Krouse, H.R. The role of organic acid in the abiogenic reduction of sulfate and the sulfur isotope effect. *Geochem. J.* **1990**, *24*, 21–27.
28. Ohmoto, H.; Rye, R.O. Isotopes of sulfur and carbon. In *Geochemistry of Hydrothermal Ore Deposits*; HL Barnes: Stratford, UK, 1979; pp. 509–567.
29. Claypool, G.E.; Holser, W.T.; Kaplan, I.R.; Sakai, H.; Zak, I. The age curves for sulfur and oxygen isotopes in marine sulfate and their mutual interpretation. *Chem. Geol.* **1980**, *28*, 199–260.
30. Leavitt, W.D.; Halevy, I.; Bradley, A.S.; Johnston, D.T. Influence of sulfate reduction rates on the Phanerozoic sulfur isotope record. *Proc. Natl. Acad. Sci. USA* **2013**, *110*, 11244–11249.
31. Habicht, K.S.; Gade, M.; Thamdrup, B.; Berg, P.; Canfield, D.E. Calibration of sulfate levels in the Archean ocean. *Science* **2002**, *298*, 2372–2374.
32. Sawicka, J.E.; Jørgensen, B.B.; Brüchert, V. Temperature characteristics of bacterial sulfate reduction in continental shelf and slope sediments. *Biogeosciences* **2012**, *9*, 3425.
33. Goldhaber, M.B.; Orr, W.L. Kinetic controls on thermochemical sulfate reduction as a source of sedimentary H_2S. In *Geochemical Transformations of Sedimentary Sulfur*; ACS Symposium Series; Vairavamurthy, M.A., Schoonen, M.A.A., Eds.; ACS Publications: Washington, DC, USA, 1995; Volume 612, 412–425. https://doi.org/10.1021/bk-1995-0612.ch023.
34. Rajabi, A.; Alfonso, P.; Canet, C.; Rastad, E.; Niroomand, S.; Modabberi, S.; Mahmoodi, P. The world-class Koushk Zn-Pb deposit, Central Iran: A genetic model for vent-proximal shale-hosted massive sulfide (SHMS) deposits–Based on paragenesis and stable isotope geochemistry. *Ore Geol. Rev.* **2020**, *124*, 103654. https://doi.org/10.1016/j.oregeorev.2020.103654
35. Jørgensen, B.B.; Isaksen, M.F.; Jannasch, H.W. Bacterial sulfate reduction above 100 C in deep-sea hydrothermal vent sediments. *Science* **1992**, *258*, 1756–1757.
36. Bradley, A.S.; Leavitt, W.D.; Schmidt, M.; Knoll, A.H.; Girguis, P.R.; Johnston, D.T. Patterns of sulfur isotope fractionation during microbial sulfate reduction. *Geobiology* **2016**, *14*, 91–101.
37. Ohmoto, H.; Kaiser, C.J.; Geer, K.A. Systematics of sulphur isotopes in recent marine sediments and ancient sediment-hosted basemetal deposits. In *Stable Isotopes and Fluid Processes in Mineralization*; Hebert, H.K., Ho, S.E., Eds.; Geological Society of Australia, Special Publication: Sydney, Australia, 1990; pp. 70–120.
38. Basuki, N.I.; Taylor, B.E.; Spooner, E.T.C. Sulfur isotope evidence for thermochemical reduction of dissolved sulfate in Mississippi Valley-type zinc-lead mineralization, Bongara area, northern Peru. *Econ. Geol*. **2008**, *103*, 783–799.
39. Ohmoto, H.; Goldhaber, M.B. Sulfur and carbon isotopes. In *Geochemistry of Hydrothermal Ore Deposits*, 3rd ed.; Barnes, H.L., Ed.; Wiley: New York, NY, USA, 1997; pp. 517–611.
40. Wilmsen, M.; Fürsich, F.T.; Seyed-Emami, K.; Majidifard, M.R.; Taheri, J. The Cimmerian Orogeny in northern Iran: Tectono-stratigraphic evidence from the foreland. *Terra Nova* **2009**, *21*, 211–218.